Jurnal Polimesin
Department of Mechanical Engineering
State Polytechnic of Lhokseumawe
http://e-jurnal.pnl.ac.id/polimesin
e-ISSN : 2549-1999 No. : 6 Month : December
p-ISSN : 1693-5462 Volume : 23 Year : 2025

Processing dates: received on 2025-9-24, reviewed on 2025-12-17, accepted on 2025-12-24 and online availability on 2025-12-31

The effect of biomass ratio and CaO/Si catalyst on hydrogen production from corncob–wood pellet gasification

Purbo Suwandono[1,*], Widya Wijayanti[2], Nova Risdiyanto Ismail[1], Dzulfikar Johan Akbar[2], Wisnu Setyo Catur Pambudi[1]
[1]Department of Mechanical Engineering, Widya Gama University, Malang 65142, Indonesia
[2]Department of Mechanical Engineering, Brawijaya University, Malang 65145, Indonesia
*Corresponding author: purbo@widyagama.ac.id

Abstract

Biomass co-gasification combined with catalytic upgrading offers a promising pathway for enhancing hydrogen-rich syngas production. This study investigates co-gasification of corncob and wood pellets in an updraft fixed-bed reactor, integrated with ex-situ CaO/Si catalytic upgrading. Nine experimental runs were conducted by varying the corncob: pellet ratio (1:1–3:1), catalyst loading (6–10 wt% of 80 g biomass), and CaO/Si ratio (1:1–3:1), while reactor geometry, inlet air speed (10 m/s), and run duration (1500 s) were kept constant. The product gas was routed through an ex-situ catalyst bed, cooled in a condenser, and then analyzed using calibrated MQ sensors (H_2, CH_4, CO, CO_2). Gas composition was monitored using calibrated MQ sensors to provide comparative trends among operating conditions. The best performance was observed in Run 7 (50:50 biomass ratio, 10 wt% catalyst, CaO/Si = 2:1), achieving peak H_2 at 8000 ppm and CH_4 at 46,000 ppm, while CO_2 decreased to 16,000 ppm compared with several other runs. This outcome was consistent with CO_2 sorption by CaO, which can shift reactions toward higher H_2 formation (e.g., via the WGS equilibrium), and was supported by downstream upgrading reactions in the hot-gas line. The results suggest that combining biomass blending with ex-situ CaO/Si upgrading can improve the characteristics of hydrogen-enriched syngas within the investigated operating range.

Keywords:
Biomass gasification, corncob, wood pellet, CaO/SI catalyst, hydrogen.

1 Introduction

Biomass gasification is increasingly considered a strategic pathway to support clean energy transition and net-zero emission targets [1]. In Indonesia, abundant agricultural and forestry residues, such as corncobs and wood pellets, offer significant potential for decentralized syngas production. However, practical deployment is still hindered by tar formation, relatively high CO_2, and a low H_2 fraction in the produced gas, which collectively reduce the usability of syngas for heat, power, or hydrogen-oriented applications [2].

A key knowledge gap remains in the experimental application of ex-situ CaO/Si catalysts for mixed-biomass co-gasification (corncob–wood pellet), particularly for improving hydrogen-enriched syngas while mitigating tar-related issues. Therefore, this study evaluates how biomass blending ratio and an ex-situ CaO/Si catalyst configuration influence syngas composition (H_2, CO, CH_4, and CO_2) and the overall upgrading performance in an updraft gasification line.

Biomass gasification converts solid feedstock into combustible syngas through coupled thermochemical steps (drying/pyrolysis, partial oxidation, and reduction), where process conditions and downstream upgrading strongly influence final gas composition [3]. Hydrogen-rich syngas is especially attractive because H_2 can serve as a low-emission fuel and an industrial feedstock, and biomass-derived hydrogen can contribute to more sustainable energy systems [4]. In this context, combining different biomass types can be beneficial: corncobs typically provide high volatile release, whereas wood pellets may offer more stable thermal behavior and a more stable bed structure during conversion, potentially producing more favorable syngas quality when co-processed.

An updraft fixed-bed gasifier is selected in this work due to its simple design, effective heat utilization, and suitability for locally available biomass resources [5]. Counter-current flow can form distinct reaction zones and enable practical operation under laboratory-scale constraints. Nevertheless, updraft gasifiers also face tar challenges, underscoring the need for an effective catalytic upgrading strategy [2].

CaO has been widely studied as a CO_2 sorbent and as a catalytic material that can promote tar cracking and shift the equilibrium toward higher hydrogen formation in sorption-enhanced schemes. By capturing CO_2 at high temperature (forming $CaCO_3$), CaO can reduce CO_2 in the gas phase and thermodynamically favor reactions associated with H_2 formation[6]. However, pure CaO is prone to sintering/agglomeration, which may reduce active surface area and sorption capacity over time [7]. To improve practicality, ex-situ catalyst placement can simplify maintenance and replacement and reduce fouling risk in the reactor. However, its experimental application—especially for mixed biomass systems—remains less reported [8].

To enhance CaO performance, silica-based supports derived from rice husk waste are attractive due to their abundance and alignment with circular-economy principles [9]. Properly treated rice husk silica can provide structural stability and surface area, thereby improving active-phase dispersion and accessibility in high-temperature environments [10]. Combining CaO with silica can yield functional synergy, where silica helps maintain catalyst structure while CaO provides CO_2 capture and tar-related upgrading functions, potentially improving hydrogen selectivity and syngas quality [11].

Accordingly, this study investigates corncob–wood pellet co-gasification coupled with an ex-situ CaO/Si catalyst to determine the effects of biomass ratio, catalyst loading, and CaO/Si composition on indicators of hydrogen-enriched syngas and CO_2 trends [12]. Beyond gas-quality improvement, the approach also supports a circular-economy pathway by transforming rice husk waste into functional catalyst-support material, contributing to more sustainable gasification technology oriented toward green hydrogen production. The novelty of this work lies in applying an ex-situ CaO/Si catalyst for corncob–wood pellet co-gasification, a configuration that has been rarely reported for mixed-biomass systems. This approach targets hydrogen-enriched syngas while leveraging rice-husk-derived silica as a circular-economy catalyst platform.

2 Research methodology

This research process was carried out at the Energy Laboratory of Widyagama University in Malang, with stages including the preparation of biomass raw materials (corn cobs and wood pellets), the preparation and impregnation of CaO/Si catalysts, the assembly and operation of a laboratory-scale gasification reactor, and the measurement of the composition of the resulting gas using analytical instruments. The entire series of activities was carried out in accordance with laboratory standard procedures, from the pre-experiment stage through the gasification process to the data processing and analysis stage, to determine the relationship

between variations in biomass ratio, catalyst loading, and CaO/Si composition on the distribution of the resulting gas.

2.1 Raw material preparation

Corncobs and wood pellets were used as the biomass feedstocks. Corncobs and wood pellets were collected from Malang Regency, Indonesia, reflecting locally abundant agricultural/forestry residues. Prior to testing, both biomasses were naturally dried (sun-drying) to reduce moisture and improve gasification repeatability. After drying, the materials were size-reduced to approximately 1 cm to obtain a more uniform bed structure and consistent gas–solid contact during fixed-bed operation.

The catalytic material consisted of CaO and rice-husk-derived silica (Si). Commercial CaO (Merck grade) was used to ensure consistent chemical quality. Rice husk silica was prepared by alkali extraction followed by acid precipitation: rice husk was treated with a dilute NaOH solution to extract soluble silicates, and the filtrate was then acidified with HNO_3 to near-neutral pH to form a silica gel precipitate. The gel was washed to remove residual ions, dried at moderate temperature, and sieved to obtain a uniform powder. The resulting silica was used as a support in the CaO/Si catalyst mixture, according to the specified CaO/Si ratio for each run.

2.2 Catalyst characterization

Rice-husk-derived silica was characterized using N_2 adsorption–desorption isotherms to validate its textural properties as a catalyst support. Measurements were performed on a Quantachrome NOVA Touch 4LX instrument. The silica sample weighed 0.1838 g and was vacuum-degassed by heating to 200°C at 10°C/min, then holding for 120 min prior to analysis. Nitrogen was used as the adsorbate at a bath temperature of 77.35 K. The specific surface area was determined using the multi-point BET method (adsorption branch), yielding a BET surface area of 314.254 m^2/g.

Fig. 1 shows the N_2 adsorption–desorption isotherm of the rice-husk-derived silica, which exhibits a progressive uptake at low-to-intermediate relative pressures, followed by a pronounced increase at high relative pressures, indicating a highly developed porous network with substantial adsorption capacity. At P/Po ≈ 0.05, the adsorbed volume is ~65 cc g^{-1}, rising steadily to ~120–150 cc g^{-1} within P/Po ≈ 0.45–0.60. A sharp uptake then occurs as P/Po approaches unity, reaching ~468 cc g^{-1} at P/Po ≈ 0.99–1.00. Such a strong high-pressure uptake is characteristic of pore-filling dominated by condensation in larger, accessible pores, consistent with an open porous architecture [11].

Notably, the desorption branch does not retrace the adsorption path, forming a distinct hysteresis loop over the intermediate-to-high P/Po region. At P/Po ≈ 0.75, the desorbed volume remains ~403 cc g^{-1} and remains elevated at ~447–460 cc g^{-1} over P/Po ≈ 0.80–0.95, before decreasing as the relative pressure is lowered. This hysteresis reflects non-identical adsorption and evaporation pathways and is typically associated with capillary condensation–evaporation processes in interconnected pore networks. Overall, the isotherm behavior—steady uptake at low-to-mid P/Po, a marked adsorption surge near saturation, and a clear hysteresis loop—supports the presence of a well-developed porous structure capable of providing high gas-accessible capacity, a desirable attribute for catalyst-support applications that require efficient gas transport and extensive interfacial contact.

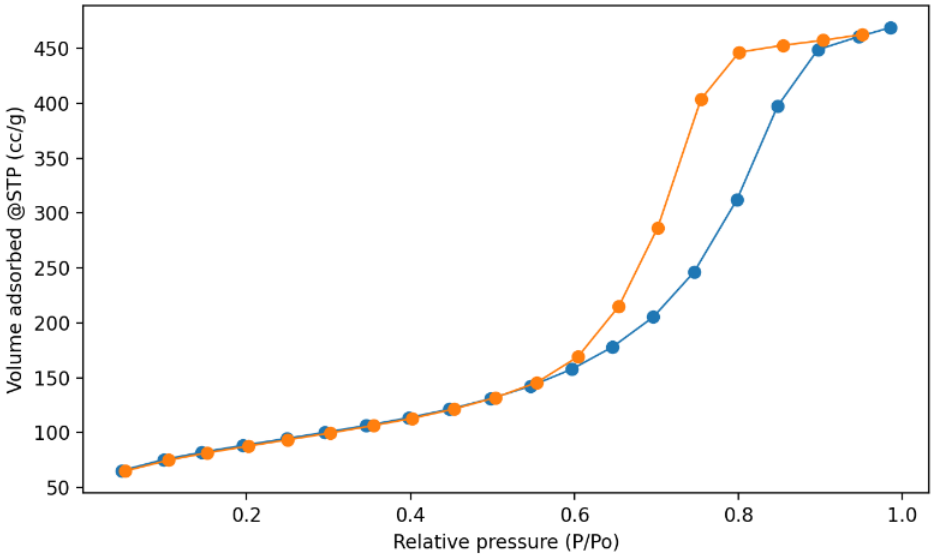

Fig. 1. Isotherm N_2 adsorption–desorption.

Fig. 2 shows the FTIR spectra (transmittance mode) clearly differentiate the functional features of the rice-husk-derived silica and CaO. For silica, a broad band centered at ~3420 cm^{-1} is observed, which is characteristic of O–H stretching from surface silanol groups (Si–OH) and/or physisorbed water on a hydroxylated silica surface. This is accompanied by a band at ~1606 cm^{-1}, commonly assigned to the H–O–H bending vibration of adsorbed water, further indicating the presence of surface hydroxylation and moisture affinity typical of porous silica [13].

The most prominent absorption feature appears at ~1109 cm^{-1}, attributable to the asymmetric stretching of Si–O–Si linkages, confirming the formation of a silica network (siloxane framework) and supporting the synthesized material's role as a robust inorganic support. A weaker feature around ~1389 cm^{-1} may arise from minor adsorbed species (e.g., residual carbonate/nitrate-related contributions from wet-chemical processing) and does not dominate the silica fingerprint compared to the strong Si–O–Si band.

In contrast, the CaO spectrum exhibits a sharp band at ~3641 cm^{-1}, indicative of O–H stretching associated with $Ca(OH)_2$, suggesting partial surface hydration of CaO upon exposure to ambient moisture. In addition, the band near ~1468 cm^{-1} is consistent with carbonate (CO_3^{2-}) vibrations, implying partial surface carbonation ($CaCO_3$) due to interaction with atmospheric CO_2. Concurrent hydration and carbonation are commonly observed in CaO-based materials and highlight the reactivity of CaO surfaces during handling and storage.

Collectively, the silica spectrum is dominated by the Si–O–Si framework band and hydroxyl-related features, reflecting a structurally stable, hydroxylated surface that can facilitate dispersion and interfacial contact when combined with CaO. Meanwhile, the CaO spectrum evidences a surface transformation to hydroxide/carbonate species, underscoring the importance of support-assisted dispersion and controlled preparation/handling for maintaining effective CaO-based functionality in catalytic upgrading applications [14].

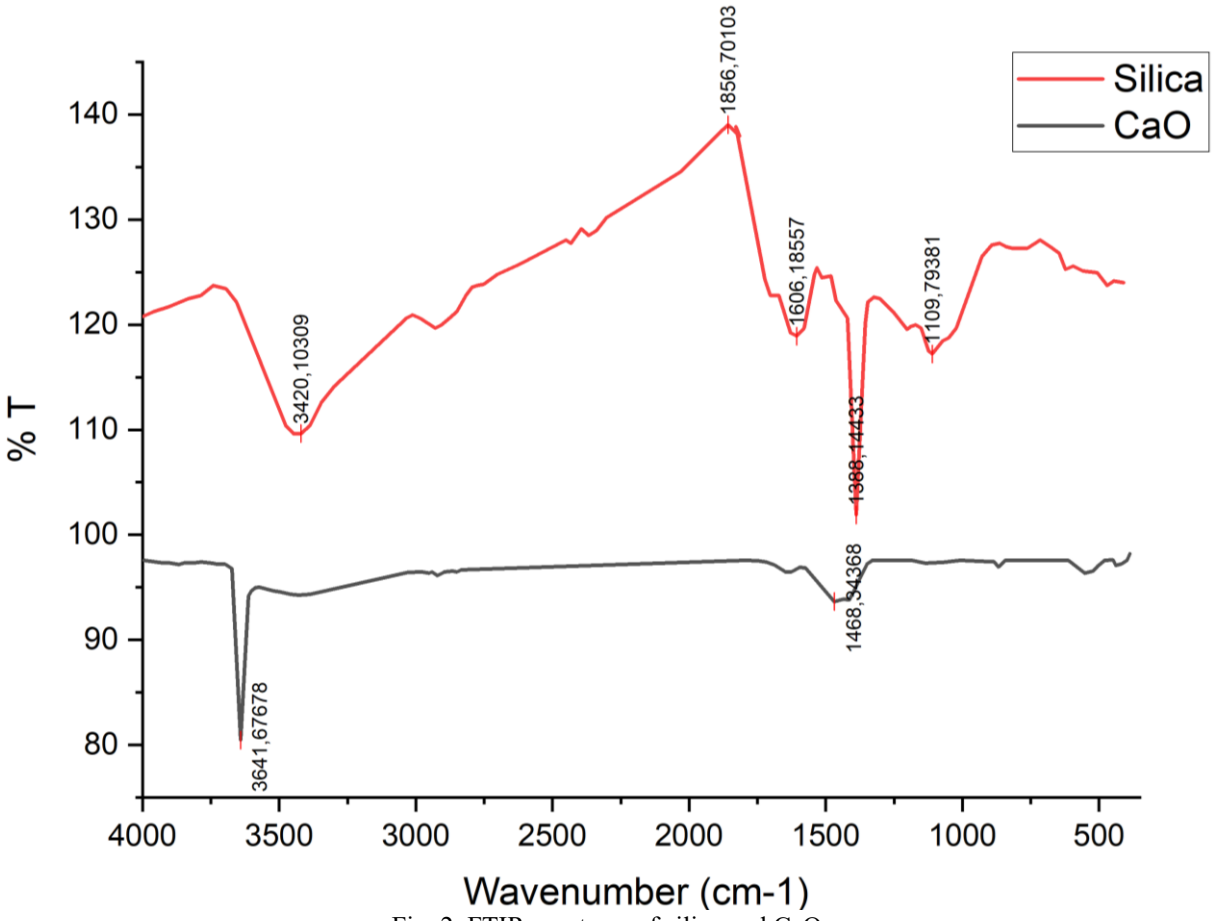

Fig. 2. FTIR spectrum of silica and CaO.

2.3 Experimental setup

This study used an updraft gasification reactor with a total height of 20 cm, as shown in Fig. 3. The lower part of the reactor consisted of an ash container 5 cm high, while the active reactor was 15 cm high and 3 inches in diameter. The reactor was equipped with a 1-inch diameter air inlet pipe connected to a blower. The blower was modified with a potentiometer to adjust air speed as needed, but in this study, the air inlet rate was kept constant at 10 m/s. To monitor the thermal conditions inside the reactor, four 3 cm long type K thermocouples were installed at several points to observe the temperature profile in the gasification zone in more detail. Each test was conducted with a fixed biomass mass, namely a mixture of corn cobs and wood pellets weighing 80 grams. The reactor was made of iron and equipped with a gas seal to prevent leaks during gasification.

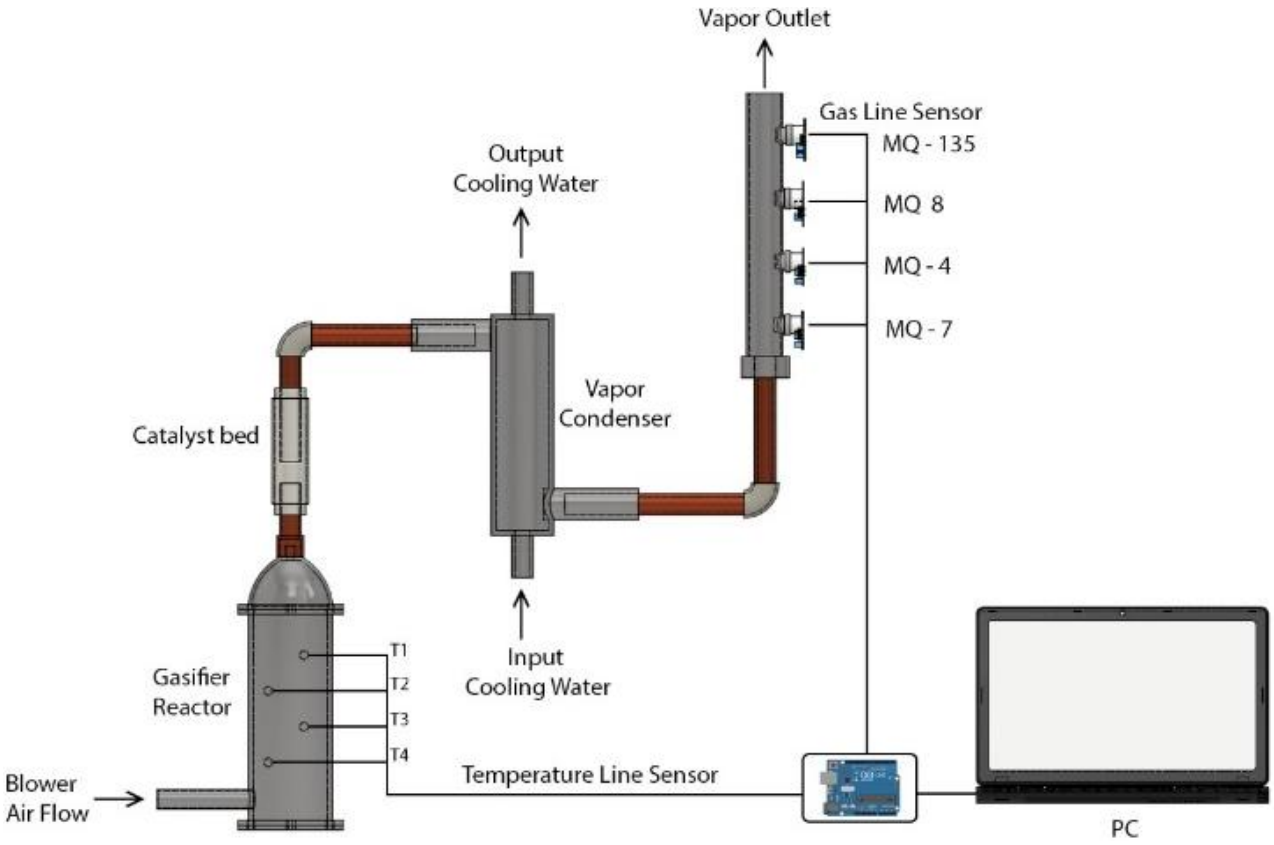

Fig. 3. Updraft gasifier experimental setup

The gas produced by the reactor was fed into a condenser, which cooled the hot gas, allowing the water vapor components to be separated. The condenser was a copper spiral pipe with a ½-inch diameter and a height of 30 cm. Cooling water was circulated from the bottom of the condenser and exited through the top to ensure efficient heat transfer. This cooling system was driven by a 60-watt water pump, ensuring stable water flow and optimal condensation.

The CaO/Si catalyst is placed ex situ, namely at the gas outlet channel from the reactor before entering the condenser. The catalyst is held in place with glass wool to maintain its desired position. The catalyst variation used is adjusted to the CaO/Si ratio specified in each experiment, so that its effect on the distribution of gasification gas can be determined.

To analyze the gas composition, four types of MQ gas sensors were used. The MQ-8 sensor was used to detect H_2, the MQ-4 for CH_4, the MQ-7 for CO, and the MQ-135 for CO_2. Each gas sensor was calibrated according to the manufacturer's datasheet, specifically by determining the Ro value, which is the sensor resistance in clean air conditions. This Ro value is used as a reference in calculating the measured gas concentration during the process.

All data from the gas sensors and thermocouples were acquired using an Arduino Uno microcontroller. Each gas sensor is connected to a separate Arduino Uno to facilitate calibration and reduce interference between sensors. Arduino is also used to record temperature data from four thermocouples installed in the reactor, enabling simultaneous measurement of gas composition and temperature distribution. Thus, this system enables real-time monitoring of reactor conditions while producing accurate data for further analysis.

2.4 Experimental operation

Nine experimental runs (Run 1–Run 9) were conducted according to the combinations summarized in Table 1, varying the corncob: wood pellet ratio (1:1, 2:1, 3:1), catalyst loading (6–10 wt% of 80 g biomass), and CaO/Si ratio (1:1, 2:1, 3:1). Each run was recorded for a fixed duration of 1500 s to capture the ignition/transient phase and to provide a consistent basis for comparing gas signals across operating conditions.

Table 1. Research data collection

Run	Corncob/pellet ratio	Catalyst loading (%)	CaO/Si ratio
1	1:1	6	1:1
2	1:1	10	3:1
3	1:1	8	2:1
4	2:1	6	2:1
5	2:1	8	3:1
6	2:1	10	1:1
7	3:1	10	2:1
8	3:1	6	3:1
9	3:1	8	1:1

For each experiment, the biomass mixture (80 g total) was charged into the updraft reactor and ignited with a torch. After ignition, the reactor was sealed to minimize leakage and maintain consistent draft conditions. The air inlet velocity was kept constant at 10 m s^{-1} for all runs. Reactor thermal behavior was monitored using four type-K thermocouples installed at different axial positions. Based on the recorded temperature profiles, the reactor reached a stable gasification regime at approximately t ≈ 200 s, at which point the temperature distribution indicated that the major gasification zones were established. Accordingly, gas-composition interpretation was focused on the post-200 s quasi-steady period, while the initial 0–200 s interval was treated as a start-up transient.

The ex-situ CaO/Si catalyst bed was installed in the outlet line upstream of the condenser and fixed using glass wool to ensure consistent packing and prevent catalyst migration. This configuration enables hot product gas to contact the catalyst before cooling, allowing upgrading reactions to proceed at elevated temperatures. To minimize variability in residence time and heat losses in the external line, the catalyst position and packing arrangement were maintained identically across all runs.

Downstream of the catalyst bed, the gas stream was cooled in a water-cooled condenser to remove moisture and reduce tar carryover. Condensed liquid and tar were separated using a gravity-assisted branching line, with the downward branch serving as a condensate/tar trap and the upward branch delivering cleaner gas to the sensing chamber. The gas composition was monitored using MQ-series sensors (MQ-8 for H_2, MQ-4 for CH_4, MQ-7 for CO, and MQ-135 for CO_2), positioned after the condenser to minimize humidity-induced drift. Each sensor was calibrated by determining Ro in clean air following the manufacturer's procedure, and signals were acquired in real time using Arduino-based logging. Potential measurement uncertainty—such as MQ cross-sensitivity, response lag, airflow fluctuations, and residual condensate/tar effects—was mitigated by: placing sensors downstream of condensation/separation, maintaining a constant airflow setting, and reporting comparative trends based on the defined quasi-steady interval rather than instantaneous start-up peaks.

Finally, note that each experimental condition was performed once; therefore, the reported results are presented as comparative indicators of performance across the tested conditions.

3 Results and discussion

3.1 Temperature distribution in the gasification zone

Fig. 4 shows the average temperature graph for runs 1-9, where all variations exhibit relatively similar thermal characteristics. Each experiment was conducted for 1500 seconds with a consistent temperature change pattern, although there were slight differences in the intensity of the temperature increase between zones. In general, the temperature curve can be divided into four main zones of the gasification process, namely the drying zone, pyrolysis zone, reduction zone, and combustion zone.

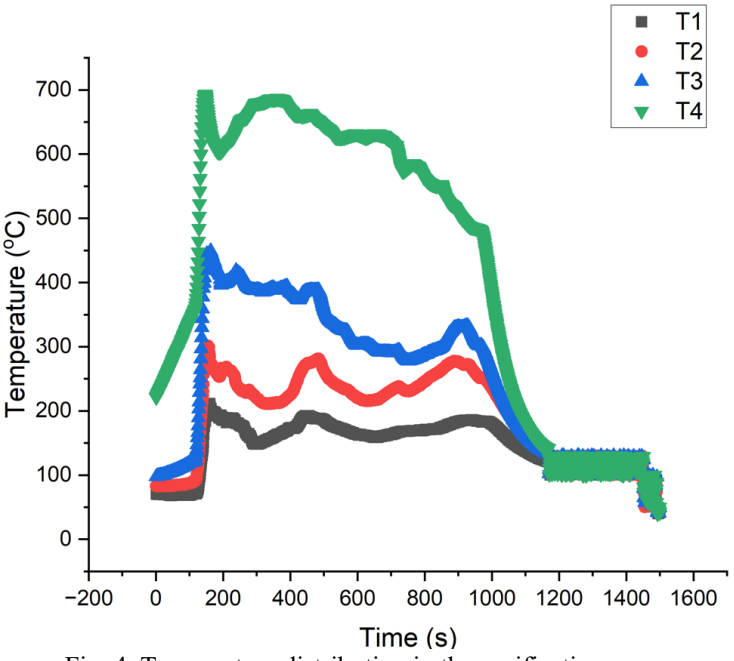

Fig. 4. Temperature distribution in the gasification zone.

The T1 curve (black) shows a relatively gradual increase in temperature from the start of the process to a range of 150–200°C. This stage represents the drying zone, where incoming heat energy primarily evaporates the water content in the biomass. The maximum temperature at this stage is around ±200°C, in accordance with the characteristics of natural moisture evaporation from biomass. The curve, which tends to be stable below the pyrolysis temperature, indicates that heat transfer is slow because most of the energy is absorbed by water vaporization rather than

directly raising the biomass temperature. A significant temperature spike begins around 200 seconds, indicating the entry of large amounts of energy from the combustion zone, which then spreads to the drying zone.

Furthermore, the T2 curve shows an increase in temperature to around ±300°C, followed by fluctuations in the range of 200–350°C. This zone is related to the pyrolysis process, which is the stage where complex organic compounds in biomass, such as cellulose, hemicellulose, and lignin, begin to decompose. This process produces volatile gases, tar, and solid carbon residue (char). The temperature fluctuations seen in the curve indicate the dynamics of volatile gas release accompanied by a combination of exothermic and endothermic reactions. At certain points, the release of volatiles triggers a rise in temperature, while at other times energy is absorbed by endothermic processes. This stage is crucial, as the quality and composition of the volatile gases formed will greatly determine the quality of the syngas produced in the next stage.

In the T3 curve, the temperature peaks at around ±450°C before gradually decreasing to around 300°C. This curve illustrates the reduction zone, where pyrolysis char reacts with CO_2, H_2O, and a limited supply of O_2 to produce CO and H_2 gases. The main reactions that occur in this zone include the Boudouard reaction ($C + CO_2 \rightarrow 2CO$) and the water–gas reaction ($C + H_2O \rightarrow CO + H_2$). The decrease in temperature after reaching the peak indicates that these reduction reactions are endothermic, thereby absorbing heat energy from the reactor environment. Thus, even as temperature decreases, the reduction zone plays an important role in forming reductive gases, the main components of syngas [15].

Meanwhile, the T4 curve shows the highest temperature spike, reaching values of over 600–700°C. This zone represents the combustion process, which is the core of the exothermic reaction in the reactor. The combustion reaction of carbon ($C + O_2 \rightarrow CO_2$) and the partial oxidation of CO gas ($CO + \frac{1}{2}O_2 \rightarrow CO_2$) release large amounts of energy, resulting in a very sharp increase in temperature. After this spike, the curve enters a plateau phase, indicating that the oxygen supply remains sufficient to sustain combustion for a period. The large amount of energy released from the combustion zone then becomes the heat source for the reactions in the pyrolysis and reduction zones. However, when the supply of fuel and air begins to decrease at around 1000–1200 seconds, the temperature in the combustion zone drops dramatically. This decrease is accompanied by a drop in temperature across all other zones, indicating the end of the active gasification phase and the start of the system cooling phase [16].

3.2 CH_4 gas composition

Fig. 5 shows that differences in raw material ratio, catalyst loading, and CaO/Si composition have a significant effect on methane accumulation. In Running 1, with a corncob/pellet ratio of 1:1, a loading of 6%, and a CaO/Si ratio of 1:1, CH_4 production was very low due to the limited number of active sites on the catalyst and the instability of its structure. These conditions prevented the tar-cracking process from operating optimally. In Run 2, increasing the catalyst loading to 10% slightly improved the results, but the CaO/Si ratio was too high (3:1), which actually favored the formation of CO and H_2, limiting CH_4 accumulation. Furthermore, in Run 3 with an 8% loading and a CaO/Si ratio of 2:1, the CH_4 yield increased to a moderate range, but was still lower than the variation with a more dominant corncob ratio.

Increasing the feedstock ratio to 2:1 in Runs 4–6 resulted in higher CH_4 yields compared to the 1:1 ratio. In Run 4 with a loading of 6%, CH_4 increased to the range of 1500–2000 ppm, indicating that the role of feedstock is critical in providing volatile compounds. However, in Runs 5 and 6, even though the loading was higher (8–10%), the unbalanced CaO/Si ratio (3:1 and 1:1) resulted in CH_4 yields that were not as high as expected. This confirms that the dominance of one component (CaO or Si) without balance actually reduces methane accumulation [17].

The most notable results were observed in Run 7, with a corncob/pellet ratio of 3:1, a catalyst loading of 10%, and a CaO/Si ratio of 2:1. These conditions yielded the highest CH_4 concentration, exceeding 3500 ppm. The dominance of corncob enriched the volatile content, while the 10% catalyst loading provided many active sites for tar cracking and partial reforming. In addition, the CaO/Si ratio of 2:1 provided an ideal balance: CaO was effective at capturing CO_2 and suppressing CH_4 oxidation, while Si maintained catalyst stability and prevented sintering. The combination of these factors creates the most thermo-chemically favorable conditions for the accumulation of large amounts of CH_4.

Meanwhile, Run 8 with the same feedstock ratio (3:1) but only 6% loading and a CaO/Si ratio of 3:1 produced lower CH_4, indicating that even though the feedstock ratio was optimal, low loading and CaO dominance reduced performance. In Running 9, although the feedstock ratio of 3:1 and loading of 8% were quite good, the CaO/Si ratio of only 1:1 was unable to maintain catalyst stability, resulting in only moderate CH_4 yields.

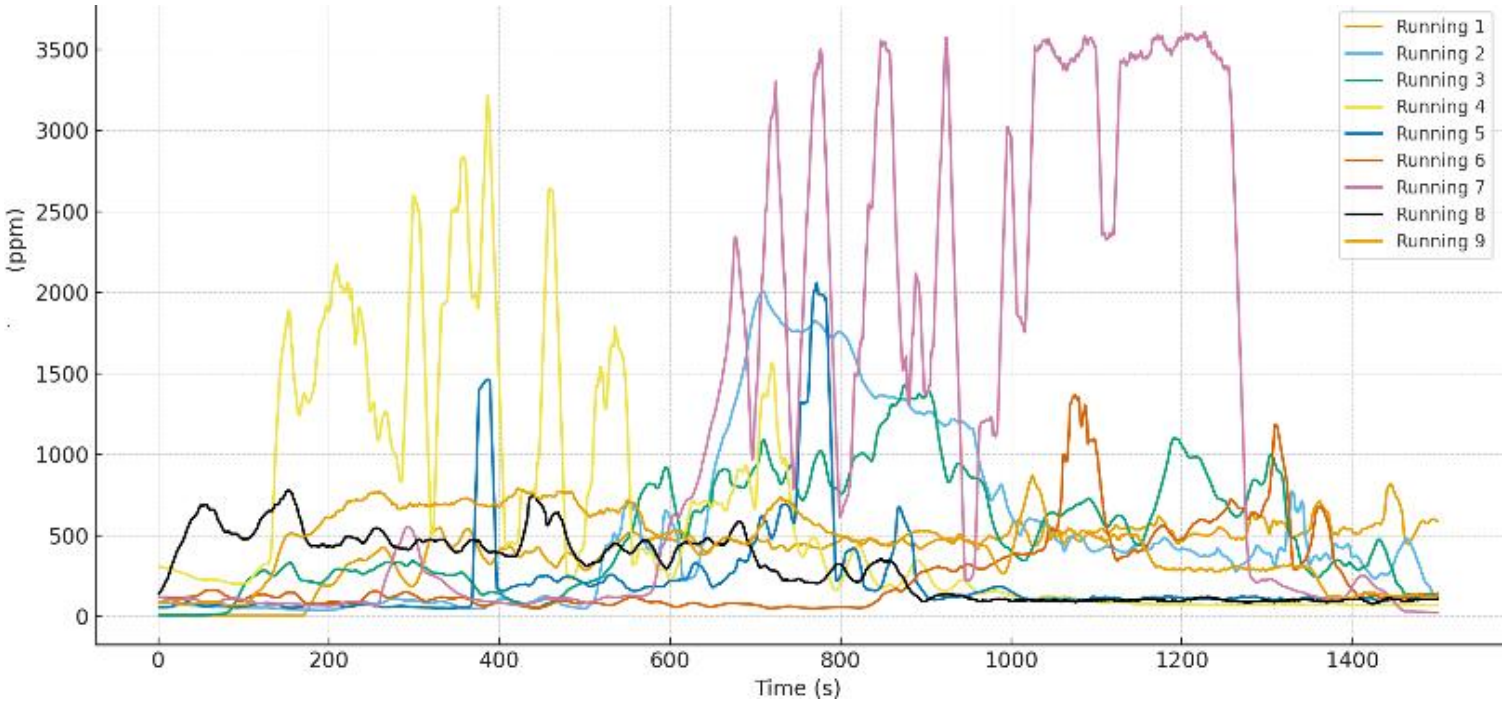

Fig. 5. CH_4 gas composition.

3.3 CO gas composition

Fig. 6 shows that the CO signal varies markedly across the nine runs, indicating that changes in biomass ratio, catalyst loading, and CaO/Si composition influence the CO formation–consumption balance. The lowest CO levels are observed in Run 1 (≤ 600 ppm) and generally lower values also appear in some 3:1 cases (Run 9, ≤ 1000 ppm). In contrast, the highest CO signals occur under the 1:1 biomass ratio with higher catalyst loading, reaching 1800–1900 ppm in Run 2 and similarly high levels in Run 3 (1800 ppm). Intermediate CO ranges are observed for the 2:1 and 3:1 biomass ratios, typically around 1100-1400 ppm, depending on catalyst loading and CaO/Si ratio (Runs 4–8).

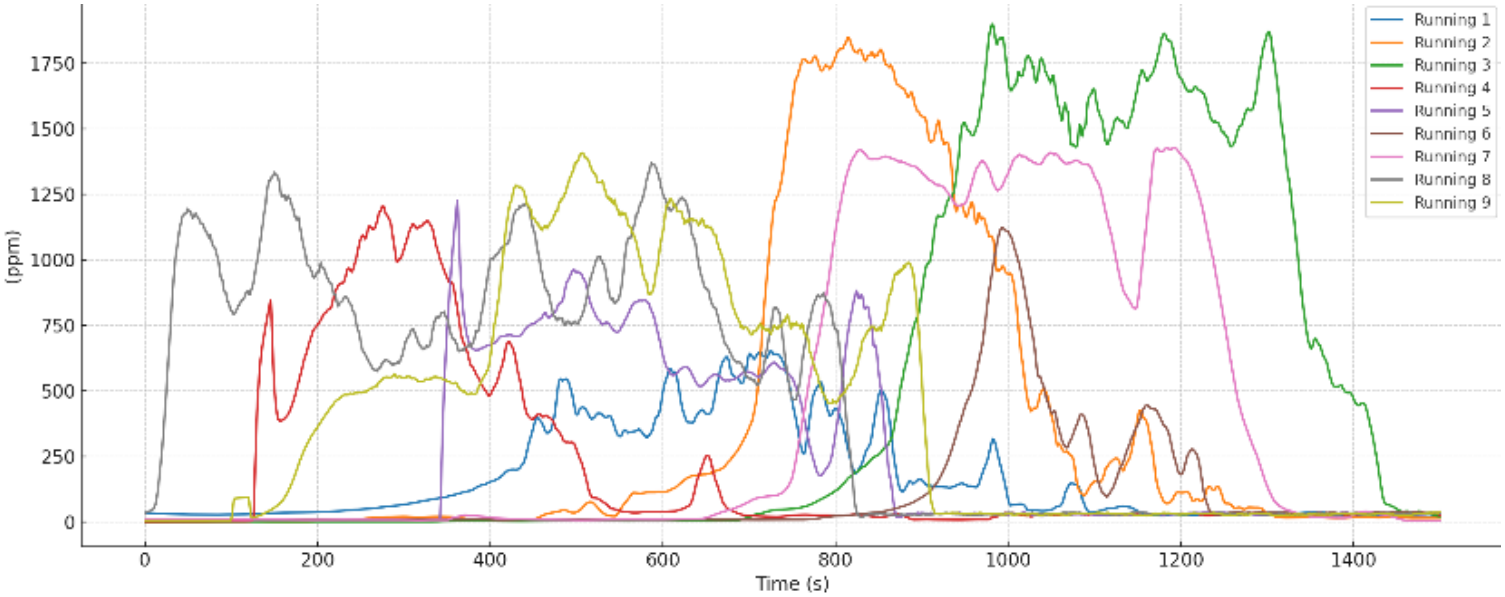

Fig. 6. CO gas composition.

CO in biomass gasification can be generated via partial oxidation and heterogeneous carbon reactions (e.g., $C + \frac{1}{2}O_2 \rightarrow CO$; $C + CO_2 \rightleftharpoons 2CO$), while it can be consumed through downstream conversion routes such as water–gas shift ($CO + H_2O = CO_2 + H_2$) and methanation ($CO + 3H_2 = CH_4 + H_2O$). Within the present dataset, the higher CO signals in Runs 2–3 are consistent with conditions that may favor CO production and/or suppress net CO consumption: higher catalyst loading can promote cracking/reforming of volatile species, and higher CaO fraction may reduce the local CO_2 level through carbonation ($CaO + CO_2 \rightarrow CaCO_3$), which can alter the CO/CO_2 balance in the upgrading line. Conversely, when the corncob fraction increases (2:1–3:1), the gas stream is expected to contain more volatiles and steam-derived species, which may enhance CO-conversion pathways (e.g., WGS and/or methanation), leading to CO signals that do not exceed the 1:1 high-loading cases even when catalyst loading is increased (Run 7).

The runs with CaO/Si = 2:1 (Runs 3 and 7) show comparatively sustained CO levels among their respective biomass-ratio groups. This trend is consistent with the role of silica as a support phase that can improve CaO dispersion and help maintain accessible reactive surface during exposure to hot product gas. However, catalyst "stability" and the dominance of specific pathways cannot be confirmed directly in the absence of dedicated deactivation tests and post-reaction characterization; therefore, these explanations are presented as plausible mechanistic interpretations rather than definitive proof.

3.4 CO_2 gas composition

Fig. 7 presents the CO_2 profiles across the nine runs and shows substantial between-run variability.

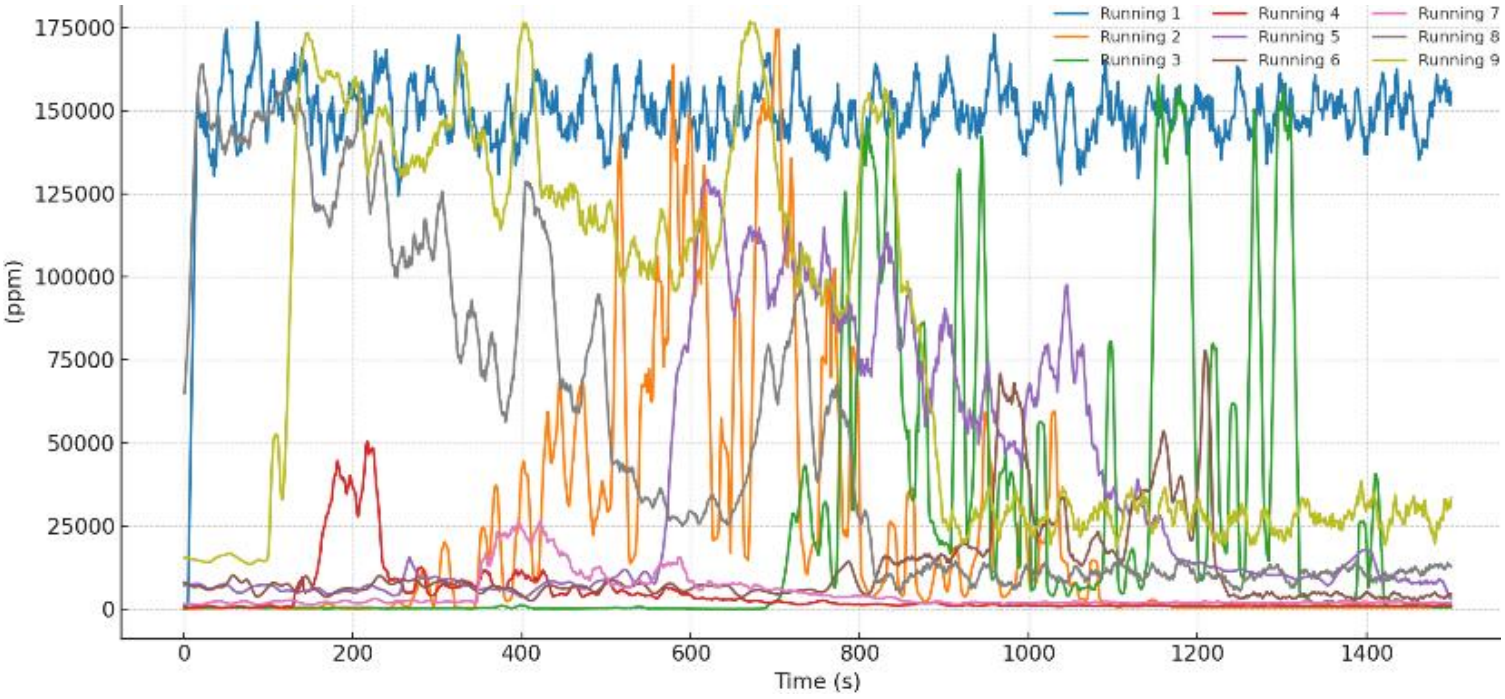

Fig. 7. CO_2 gas composition.

Under the 1:1 biomass ratio group, CO_2 signals are generally high, with Run 1 remaining at the upper range (reported >150,000 ppm) and Runs 2–3 showing lower but still elevated CO_2 levels (approximately 120,000–140,000 ppm). For the 2:1 group (Runs 4–6), the CO_2 signal remains high and fluctuating in several cases, whereas Run 6 exhibits comparatively lower CO_2 (approximately 60,000–80,000 ppm). A distinct behavior is observed in the 3:1 group, where Run 7 shows a markedly lower CO_2 signal (<20,000 ppm) compared with the other runs, while Runs 8–9 return to moderate-to-high ranges [18] [19].

In an ex-situ CaO/Si upgrading line, CO_2 trends can be influenced by two coupled effects: net CO_2 formation from oxidation and downstream conversion reactions, and CO_2 removal via carbonation ($CaO + CO_2 \rightarrow CaCO_3$) when CaO is available and accessible [20]. Within the present dataset, the reduction of CO_2 from Run 1 to Runs 2–3 is consistent with increased sorbent availability at higher catalyst loadings and higher CaO fractions. For the 2:1 biomass ratio group, higher volatile release and steam-derived species may enhance CO/CO_2 inter-conversion reactions, which can contribute to fluctuating CO_2 profiles; however, without gas-phase kinetic measurements or direct steam quantification, this remains a plausible interpretation rather than a definitive conclusion.

The notably low CO_2 in Run 7 coincides with the condition that also yielded high H_2/CH_4 signals in the study. A plausible explanation is that CO_2 was more effectively removed/converted under this setting due to the combined effects of an ex-situ bed composition that maintained CO_2 uptake capability (CaO presence with silica acting as a stabilizing/dispersing phase), and a gas environment richer in reducing species from the higher corncob fraction that may shift the apparent CO/CO_2 balance.

3.5 H_2 gas composition

The measurement results show that variations in biomass ratio, catalyst loading, and CaO/Si composition significantly affect H_2 formation. In Run 1 with low loading (6%) and a CaO/Si ratio of 1:1, H_2 production was relatively small due to limited reforming and CO_2 absorption capacities. Running 2 and Running 3 showed an increase in H_2, with higher loadings (10% and 8%) and the presence of dominant or balanced CaO promoting steam reforming and water–gas shift reactions. However, the CO_2 content was still quite high, so H_2 formation was not maximized. In Running 4–6, a larger biomass-to-water ratio (2:1) increases the release of volatiles and water vapor, thereby increasing H_2 production, although production stability is highly dependent on catalyst effectiveness. An unbalanced CaO/Si ratio or a too-low loading makes reforming unsustainable (Fig. 8).

The most notable phenomenon occurs in Running 7, with gas levels reaching 8000 ppm. Under these conditions, the H_2 concentration surged to its highest value among all runs. Several factors caused this increase. First, the CaO/Si ratio of 2:1 provided ideal synergy: CaO effectively absorbed CO_2, while Si maintained dispersion and prevented sintering, thereby preserving the active surface area. This CO_2 absorption reduces the CO_2 concentration in the gas, and according to Le Chatelier's principle, drives the steam reforming reaction ($C + H_2O \rightarrow CO + H_2$, $CH_4 + H_2O \rightarrow CO/CO_2 + H_2$) and the forward water–gas shift ($CO + H_2O \rightarrow CO_2 + H_2$) further towards the H_2 product. Second, the 3:1 biomass ratio dominated by corncobs enriches the supply of volatiles and water vapor, providing more reactants for H_2 production. Third, the 10% catalyst loading provides the maximum number of active sites to support these reactions [21].

These conditions explain why Running 7 saw a very significant increase in H_2, while the CO_2 graph showed a sharp decline. Carbon that should have been released as CO_2 was instead converted into reductive gases, particularly H_2 and CH_4, shifting the product distribution towards more energy-rich gases. In Run 8, the H_2 concentration increased rapidly at the beginning, peaking at around 4000 ppm, but then declined sharply and became unstable. This was due to a combination of a dominant corncob feed (3:1), which produced a lot of volatiles and steam, and a very high CaO/Si ratio of 3:1 in CaO. The dominance of CaO is indeed effective in reducing CO_2 at the beginning and triggering H_2 formation through reforming and water–gas shift reactions, but the low catalyst loading (6%) limits the number of active sites [22]. As a result, catalyst activity quickly saturates and declines, preventing H_2 concentrations from remaining high in the long term. Running 9 produces H_2 at a moderate level (2000–3000 ppm), with a fluctuating pattern. The 3:1 feed ratio enriches the volatile and vapor content, making the reforming reaction quite active. However, a CaO/Si ratio of 1:1 is not optimal for maintaining CaO dispersion, leading to a decrease in active surface area due to sintering tendencies. With an 8% loading, the catalyst activity is indeed better than Running 8, but it cannot match the stability and effectiveness seen in the 2:1 ratio (e.g., Running 7). As a result, a sufficient amount of H_2 is formed, but it does not reach a high peak and persist for a long time as in Running 7.

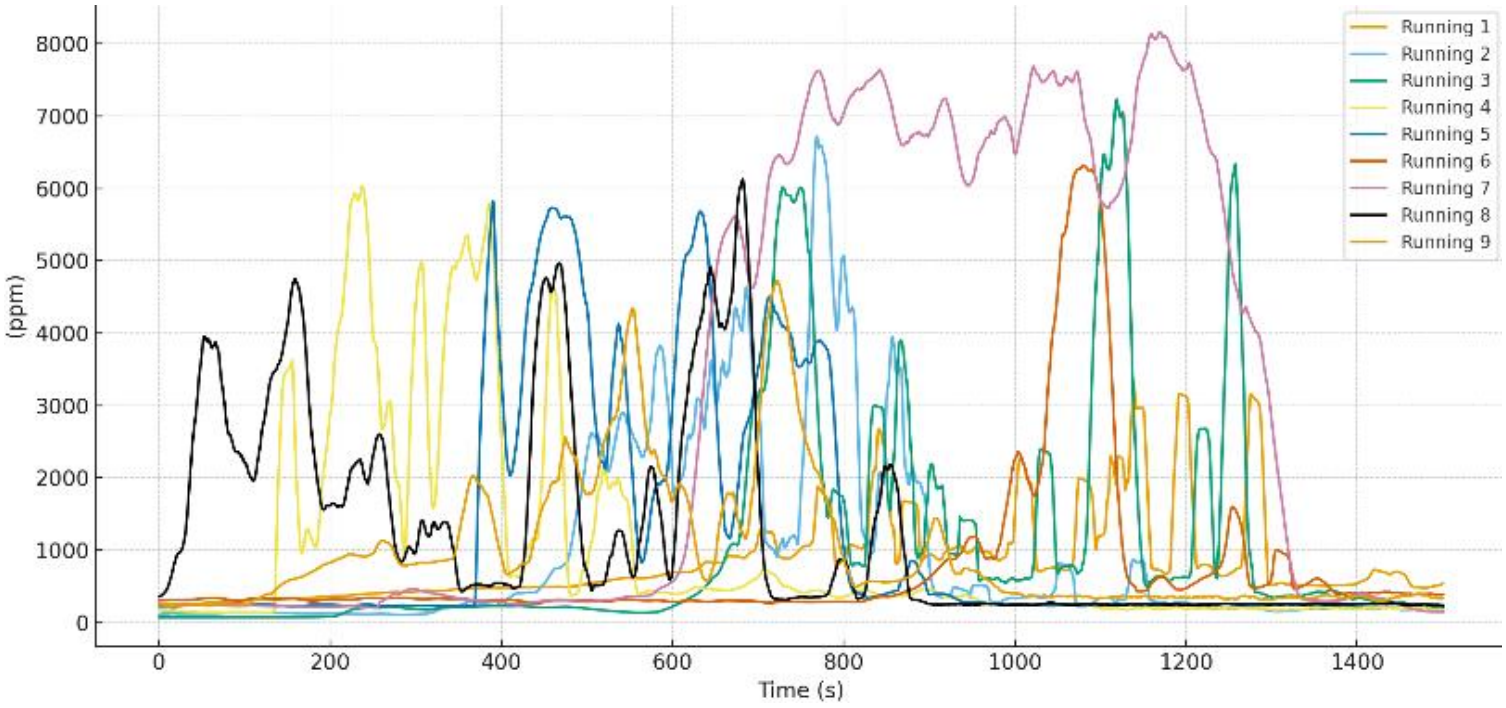

Fig. 8. H_2 gas composition.

4 Conclusions

This study demonstrates that the corncob-wood pellet blending ratio, catalyst loading, and CaO/Si composition significantly influence syngas indicators in an updraft co-gasification line equipped with an ex-situ CaO/Si upgrading bed. Increasing catalyst loading generally improved gas upgrading performance, with the highest loading tested (10 wt%) producing the most favorable overall trends. Among CaO/Si formulations, a 2:1 ratio provided the most balanced response, consistent with silica's role as a support phase that helps maintain accessible CaO functionality. Within the investigated range, the best overall condition was Run 7 (corncob: pellet 3:1, catalyst loading 10 wt%, CaO/Si 2:1), which simultaneously delivered the highest observed H_2 (~8000 ppm) and CH_4 (~46,000 ppm) signals while showing a markedly lower CO_2 trend compared with most other runs. These results support the main contribution of this work showing that mixed-biomass co-gasification combined with ex-situ CaO/Si upgrading can significantly enhance hydrogen-enriched syngas characteristics and optimize carbon distribution.

References

[1] M. Buffi, M. Prussi, and N. Scarlat, "Energy and environmental assessment of hydrogen from biomass sources: Challenges and perspectives," Biomass and Bioenergy, vol. 165, p. 106556, 2022.

[2] A. S. Al-Rahbi and P. T. Williams, "Hydrogen-rich syngas production and tar removal from biomass gasification using sacrificial tyre pyrolysis char," Appl. Energy, vol. 190, pp. 501–509, 2017.

[3] J. Kumar and S. Vyas, "Comprehensive review of biomass utilization and gasification for sustainable energy production: Comprehensive review of biomass utilization and gasification...: J. Kumar, S. Vyas.," Environ. Dev. Sustain., vol. 27, no. 3, 2025.

[4] R. Hidayat, P. Suwandono, W. S. C. Pambudi, and H. D. Saputra, "Peningkatan Peforma Design Gasifier Tipe Downdraft Dengan Variasi Jumlah Aliran Udara," AL JAZARI J. Ilm. Tek. MESIN, vol. 10, no. 1, 2025.

[5] Y. Tangke Tosuli, Cahyadi, H. Dafiqurrohman, R. Hermawan, and A. Surjosatyo, "Gasification of sago dreg waste in a top-lit updraft fixed bed gasifier: Syngas composition and its effect with additional Al2O3 as catalyst," Energy Convers. Manag. X, vol. 24, no. October, p. 100775, 2024, doi: 10.1016/j.ecmx.2024.100775.

[6] R. Liu, C. Li, J. Zheng, F. Xue, M. Yang, and Y. Zhang, "Hydrogen-rich syngas production via sorption-enhanced steam gasification of biomass using FexNiyCaO bi-functional materials," Energy, vol. 281, p. 128269, 2023.

[7] T. Bunma, "Synergistic study between CaO and MgO sorbents for hydrogen-rich gas production from the pyrolysis-gasification of sugarcane leaves," Process Saf. Environ. Prot., vol. 118, pp. 188–194, 2018, doi: 10.1016/j.psep.2018.06.034.

[8] H. Yang, "The effect of CaO on coal gasification reaction with high-temperature copper slag as catalyst," Energy Sources, Part A Recover. Util. Environ. Eff., vol. 45, no. 3, pp. 9450–9464, 2023, doi: 10.1080/15567036.2023.2239745.

[9] Y. Wang, L. Huang, S. Li, C. Liu, and H. He, "The Capture and Catalytic Conversion of CO2 by dendritic mesoporous silica-based nanoparticles," Energy Environ. Mater., vol. 7, no. 2, p. e12593, 2024.

[10] Z. Li, S. Das, P. Hongmanorom, N. Dewangan, M. H. Wai, and S. Kawi, "Silica-based micro-and mesoporous catalysts for dry reforming of methane," Catal. Sci. Technol., vol. 8, no. 11, pp. 2763–2778, 2018.

[11] I. Hamidu, B. Afotey, B. Kwakye-Awuah, and D. A. Anang, "Synthesis of silica and silicon from rice husk feedstock: A review," Heliyon, vol. 11, no. 4, 2025.

[12] X. Wang, W. Zeng, C. Xin, X. Kong, X. Hu, and Q. Guo, "The development of activated carbon from corncob for CO2 capture," RSC Adv., vol. 12, no. 51, pp. 33069–33078, 2022, doi: 10.1039/d2ra05979g.

[13] L. Bünger, K. Garbev, A. Ullrich, P. Stemmermann, and D. Stapf, "Mixed-Matrix Organo-Silica–Hydrotalcite Membrane for CO2 Separation Part 1: Synthesis and Analytical Description," Membranes (Basel)., vol. 14, no. 8, p. 170, 2024.

[14] X. Wei et al., "Synthesis of large mesoporous silica for efficient CO2 adsorption using coal gasification fine slag," Sep. Purif. Technol., vol. 353, p. 128348, 2025.

[15] Z. Chen, Y. Liao, Y. Chen, and X. Ma, "Insight into the gas pollutants emission of rural solid waste during the gasification-combustion process: Influencing factors and mechanisms," Fuel, vol. 355, p. 129510, 2024.

[16] M. Hamdy, M. El-Adawy, and M. A. Nemitallah, "Optimizing in-situ combustion gasification for enhanced clean hydrogen production with in-situ CO2 sequestration," Case Stud. Therm. Eng., p. 106440, 2025.

[17] B. Luo, Y. Su, X. Ding, Y. Chen, and C. Liu, "Modulation of initial CaO/Al2O3 and SiO2/Al2O3 ratios on the properties of slag/fly ash-based geopolymer stabilized clay: Synergistic effects and stabilization mechanism," Mater. Today Commun., p. 113295, 2025.

[18] M. Chen et al., "Sulfate residuals on Ru catalysts switch CO2 reduction from methanation to reverse water-gas shift reaction," Nat. Commun., vol. 15, no. 1, p. 9478, 2024.

[19] H. Song, X. Zhang, X. Lin, H. Bian, and Y. Liu, "Process analyses on sorption-enhanced electrified steam methane reforming for near-zero emission hydrogen production with CO2 capture by calcium looping thermochemical reaction," Appl. Energy, vol. 385, p. 125537, 2025.

[20] Y. Zhang, H. Liu, J. Lu, Q. Xu, and C. Xu, "An integrated energy storage system coupling Ca (OH) 2/CaO/CaCO3 thermochemical energy storage, supercritical CO2 cycle, and CO2 capture," J. Energy Storage, vol. 130, p. 117487, 2025.

[21] T. Tuntiwongwat, T. R. Srinophakun, and S. Sukpancharoen, "Computational thermodynamic analysis of hydrogen production via biomass gasification," in 2024 International Conference on Advanced Robotics and Mechatronics (ICARM), IEEE, 2024, pp. 715–720.

[22] Y. Zhou, X. Ma, Q. Yusanjan, H. Cui, Z. Cheng, and Z. Zhou, "Active metal-free CaO-based dual-function materials for integrated CO2 capture and reverse water–gas shift," Chem. Eng. J., vol. 485, p. 149937, 2024.